



---

# Audio Engineering Society

# Convention Paper

Presented at the 121st Convention  
2006 October 5–8 San Francisco, CA, USA

*This convention paper has been reproduced from the author's advance manuscript, without editing, corrections, or consideration by the Review Board. The AES takes no responsibility for the contents. Additional papers may be obtained by sending request and remittance to Audio Engineering Society, 60 East 42<sup>nd</sup> Street, New York, New York 10165-2520, USA; also see [www.aes.org](http://www.aes.org). All rights reserved. Reproduction of this paper, or any portion thereof, is not permitted without direct permission from the Journal of the Audio Engineering Society.*

---

## Stress Analysis on Moving Assemblies and Suspensions of Loudspeakers

Fernando Bolaños

Acústica Beyma S.A., Valencia, 46113, Spain

### ABSTRACT

The paper explains the basic results of numerical and experimental analysis of moving assemblies and suspensions of speakers taking into account the bending forces and the in plane forces that acts on these slender bodies. The distribution of these stresses is shown in cones of direct radiators and in domes (for example, in compression drivers) as well. An explanation of the generation of subharmonics is obtained by this technique. The sudden jump of the working point on moving assemblies is justified by means of the compression forces that act on the suspensions. These compression forces are the cause of the buckle or snaps that very often occur in the speakers. This article analyzes different types of suspension showing the compromising situation the designer has to deal with.

### 1. PURPOSE AND INTRODUCTION

The intention is to do an overview of the normal stresses in the moving assembly, and to have the minimum necessarily knowledge to start the design of suspensions in loudspeakers. The problem of deformations of the moving assembly and suspensions is regularly treated by modal analysis, but unfortunately, much less attention is paid to the stress distribution in these parts of the speakers. The stress distribution along the moving parts shows the

main nature of the loads carried by the elements that build up in the transducer. A stress reduction is convenient both in the moving assembly and the suspensions; as, the normal modes will be less stress dependent, the potential traveling waves will move free on the cone, the moving assembly will move smoothly, and hence, the transducer will radiate better sound.

Before beginning to look at the design from the point of view of the dynamics (modal analysis), it is convenient to apply static load to the coil and analyze the stress and strain response. The static analysis gives an insight of the information of the performance of all elements in motion, not only in

respect to the stiffness but also in respect to the nature of the internal loads and the amount of bending and in plane stresses on all the transducer.

In loudspeakers the use of very soft materials is common, such as the resinous technical textiles and foams for suspensions, and the use of hard materials like the polyester, titanium, etc. is also common. These materials behave very differently, while the firsts ones acts as nonlinear soft, the lasts behaves nonlinear hard. This circumstance implies a plurality of performance combinations in practice.

### 1. 1. The tensile and compressive stresses in thin shells.

Following the criteria given by the professor Den Hartog [1] the use of two orthogonal coordinates are the most simply to handle shells of revolution, these coordinates are the meridional and the tangential coordinates. The meridional coordinate is the length of the shell measured along a meridian, this is called longitudinal as well. The tangential is the measure of the length of the sell along a parallel or a hoop. Figure 1 depicts these coordinates in a shell.

If the shell is loaded some parts of it will resist extension loads, and some parts resist compression loads. The transition between extension and compression is a region where the elements have a high shape distortion and the forces are of shear nature.

Figure 2 depicts an element of a cylinder shell subjected to extension forces in both meridional and tangential directions. If the opposite arrows were rotated  $\pi$  radians each, the element would be submitted to compression in the two coordinates. Both extensional and compression forces are very different in character. In a technical textile the resinous textile material performs well in extension but not in compression. The fabric do not support these compression loads. This point will be seen later in depth.

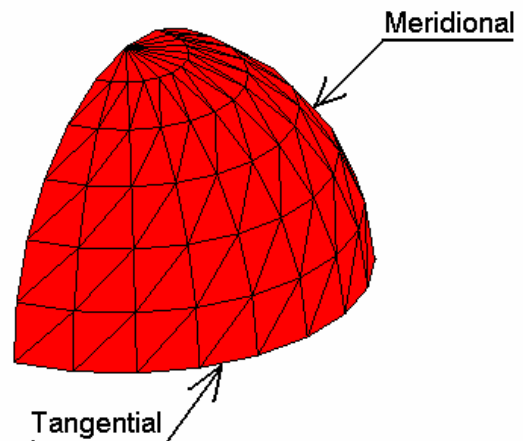


Figure 1: Meridional and tangential coordinates on a shell.

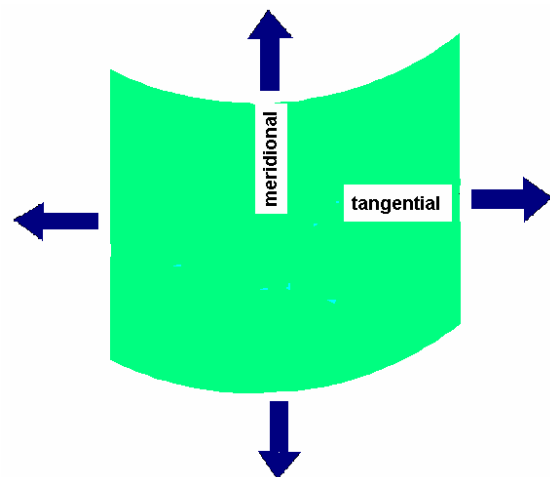


Figure 2: Cylinder shell element submitted to extensional forces in both coordinates.

When a shell is submitted to bending it will develop a stress due to this deformation; if the shell is submitted to a load in plane, there will be in plane stress and strain as well. These bending and in plane

are the two kind of stresses and strains that the shell will carry.

Assume we have a hose which has a cross section in the form of an ellipse because it has been deformed (flattened) for some reason. If pressure is applied to the hose, a small amount of it will be sufficient to obtain the original cross section which is a circle. But if we want to inflate the hose and obtain a circular cross section of bigger radius, much more pressure is needed. The first mild pressure that retrieves the original circumference cross section applies bending stress to the hose. The additional pressure is held by the hose wall by in plane stress. This simple example applies to other slender bodies as the suspension. The first action in a deformed suspension is bending, after it, the in plane forces acts on the body subjected to any kind of load, pressure or force.

The stresses measured on two orthogonal coordinates are not equal. In a cylinder we have:

$$S_t = p \times r_0 / t \quad (1)$$

$$S_m = p \times r_0 / (2t) \quad (2)$$

Being  $S_t$  and  $S_m$  the tangential and meridional stresses respectively,  $p$  is the applied pressure,  $t$  is the thickness of the cylinder wall, and  $r_0$  is the radius of the cylinder. Moreover  $c = 1/r_0$  is the curvature of the cylinder.

The tangential stress is double than the meridional (longitudinal) stress. This is a consequence of the fact that:

$$(S_m / R_m) + (S_t / R_t) = p / t \quad (3)$$

and  $R_m$  is infinite for a cylinder.

The topic of strength of materials can be revised for example in [2] and [3], the study of shells can be seen for example in [4] and [5], the general theory of matrix structural analysis in references [6] and [7]. and the theory of stability of structures in [8], among many others.

The in plane stress in a shell element at which external pressure is applied is calculated based on the following formulas:

$$\partial S_x / \partial x + \partial S_s / \partial y = 0 \quad (4)$$

$$\partial S_y / \partial y + \partial S_s / \partial x = 0 \quad (5)$$

And the equation (3), written on Cartesian coordinates yields:

$$(S_x / R_x) + (S_y / R_y) = p / t \quad (6)$$

Being  $S_x$  and  $S_y$  the longitudinal and transversal stresses on the element and  $S_s$  is the shear stress. The shear stress deforms a rectangle element into a trapezium.

The basic equations for a shell element in bending are:

$$M_x = D(\partial^2 w / \partial x^2 + \mu \partial^2 w / \partial y^2) \quad (7)$$

$$M_y = D(\partial^2 w / \partial y^2 + \mu \partial^2 w / \partial x^2) \quad (8)$$

$$T_{xy} = D(1 - \mu) \partial^2 w / \partial xy \quad (9)$$

Being :

$M_x$  and  $M_y$  the bending moments on the element in the x and y directions,  $T_{xy}$  is the twisting torque on the element,  $w$  is the displacement normal to the element,  $D$  is the bending stiffness of the shell and

has the value:  $D = \frac{Et^3}{12(1 - \mu^2)}$  (10), and finally,  $\mu$

is the Poisson ratio.

The equations (7), (8) and (9) are equivalent to the equation:

$M = EI * y''$  (11) in beam theory (where  $EI$  is the bending stiffness of the beam). Extensive explanations of this topic are available on references [2] and [3], for example.

Here we will deal with slender bodies of some stiffness like the cone and a stiff dome of a compression driver, and later we will treat slender bodies of less stiffness as the suspensions.

## 2. THE STRESSES ON A CONE

In mechanics it is well known, that the main eigenvector of a slender structure has the same shape that the structure has due to the load of its own weight. This propriety has been very helpful for the analysis of large structures and rotors, for example. In this engineering field the slender rotors bends because of its own dead weight. The deformed body must satisfy the boundary conditions which are imposed by the bearings. This is the case of a loudspeaker as well. A static load applied to the coil, gives a static deformation of the full moving assembly, which corresponds with the main speaker mode, which obviously, is only axial. This justifies the use of the statics in the speaker analysis. If we deal with modes of higher frequency, the situation is very similar. For example, the high frequency axial modes of the moving assembly, of which there are two, can be found simply extending the coil's load just at the end of the speaker stroke. Then the moving assembly will deform axially. Thus the two axial modes will appear, showing the elasticity near the cone rim and near the moving assembly neck, see reference [9]. This static deformation is the base to understand the dynamic axial mode shapes.

But the most convenient way to observe the stresses on a cone is to suspend the moving assembly by means of a set of ideal suspensions both in the cone rim and the neck as it is done in practice. The ideal suspension is a device formed by an orthogonal set of springs of equal stiffness, providing isotropic conditions. In the proposed FEM model each node of the rim and each one of the neck has a boundary condition of three equal translational springs and three equal rotational springs as well. Because the main object is the knowledge of the linear behavior, the ideal suspensions are set up of the soft type. This soft type suspension agrees well with most real transducers.

This procedure will provide the stress distribution, basically due to the cone geometry and due to the materials used. In practice other stresses, like the ones exerted by the real suspensions, will be added to those which belong to the cone itself.

We must notice that principal stresses are the maximum values that compression, tension and shear can take on as we look at the reference block (element) as it is rotated through an angle. The  $S_1$  and  $S_2$  normal stress values are at a rotation angle where the shear stress is minimum. So that the  $S_1$  and  $S_2$  stresses are taken in a set of orthogonal directions established by the condition of less shear stress. The present value of shear stress is the highest value of shear which occurs at an angle where the normal stresses are equal and at a value  $(S_1+S_2)/2$ , see the references [1], [2] and [3].

The Figure 3 depicts a modeled moving assembly and the upward applied load at the coil. The elements are oriented in a local set of coordinates, the meridional  $X$  and the tangential  $Y$ . In our case of revolution's symmetry, this local set of coordinates corresponds roughly with the principal stresses axis  $S_1$  and  $S_2$ .

One of the two principal cone stresses, the called  $S_1$ , is depicted in the figure 4. The coil and the former are omitted for clarity. The scale at left side for this figure and all the rest in the paper are in relative values. Observe that the cone rim performs in tension by a positive magnitude, while the cone neck, for this particular direction, performs in compression (which is negative). The other principal stress  $S_2$ , which is depicted on the Figure 5, has the same trend, except that the tension on cone rim is higher than the  $S_1$  (see the score at left side).

If a cone area has a surface in tension and an adjacent surface in compression, then, between the areas subjected to opposite stress, will be a zone of shear stress, which is depicted in the Figure 6. The shear stress is concentrated on a ring of shorter radius than the radius of tensile stress on the rim. There is another shear area of less strength near the cone neck.

Table 1 illustrate the stress values  $S_1$  and  $S_2$  in the cone taking into account the mathematic terms of both types of stresses and strains in the cone (bending and in plane), or the mathematic terms due to the bending alone. These values must be managed with caution, and must be treated as a whole set. Despite the fact that the minimum strength of  $S_2$  when only applying the bending terms is lower than the corresponding when all terms are used, the results are consistent. An overview of the table shows that the stress  $S_1$  is noted to have a contribution of both type of strains, the bending and the in plane, both in tension and in compression. However the strength of  $S_2$  has the same trend as that of  $S_1$  for tensile stress,

but in terms of compressive stress, S2 is much higher using only the bending terms rather than all terms, which means that bending stress is more influential than in-plane stress. This is due to the presence of the former and coil. The shear stresses pattern, which is illustrated on figure 6, shows that where there are high changes of the principal stresses from tensile to compression and vice versa a high shear stress is developed. These regions are close to the cone rim and close to the cone neck.

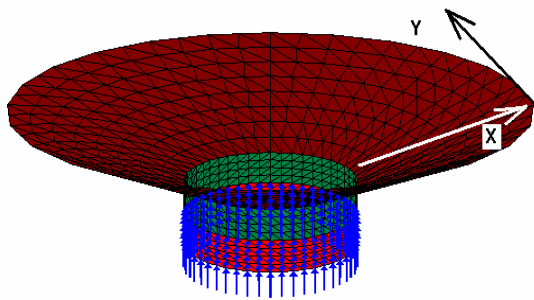


Figure 3: Moving assembly with positive load on the coil and a detail of local coordinates.

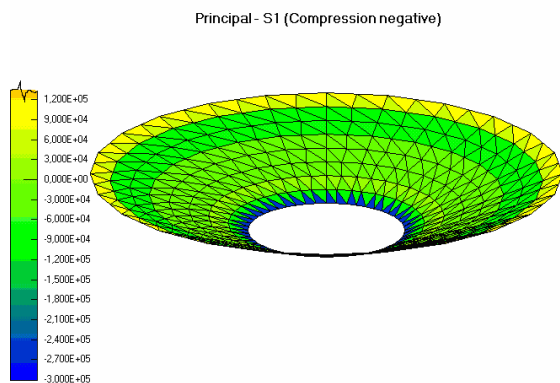


Figure 4: Principal Stresses S1 on the cone. Scale on left must be taken as relative values. Scale is arranged for black and white print. Colors not appearing at the cone as been erased on the scale.

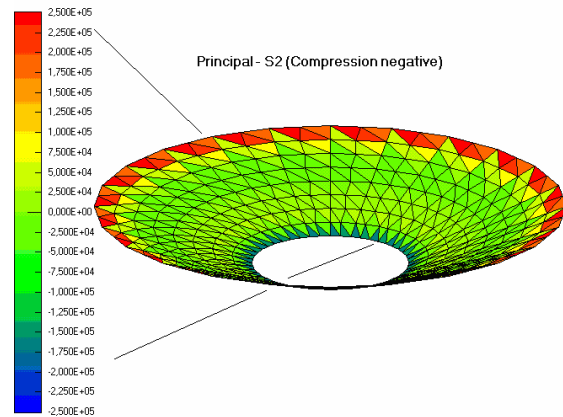


Figure 5: Principal Stresses S2 on the cone

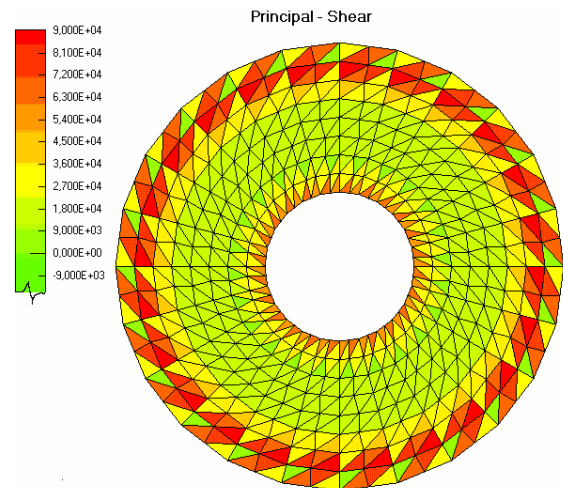


Figure 6: Shear on the cone

| Terms used on calculations | Principal stress axis | Max. strength (tensile) | Min. strength (compressive) |
|----------------------------|-----------------------|-------------------------|-----------------------------|
| All terms                  | S1                    | 1.14e5                  | -2.7e5                      |
| All terms                  | S2                    | 2.36e5                  | -1.66e5                     |

|                     |           |               |                |
|---------------------|-----------|---------------|----------------|
| <i>Only Bending</i> | <i>S1</i> | <i>6.07e4</i> | <i>-1.28e5</i> |
| <i>Only Bending</i> | <i>S2</i> | <i>1,51e5</i> | <i>-3.65e5</i> |

Table 1

S1 and S2 components of the cone stresses, based on calculations with all terms or only with the bending terms. Take the values as relatives between them.

### 3. THE STRESSES ON A DOME AND SUSPENSION OF A COMPRESSION DRIVER.

Figure 7 depicts the dome of a compression driver, which is a spherical segment, and illustrates the meridional and tangential coordinates. Figure 8 depicts the complete moving assembly with its suspension, which is flat.

If we apply pressure to a sphere, both stresses  $S_m$  and  $S_t$  will be equal, and have the magnitude:  $S_m = S_t = pr_0 / (2t)$  (12). The sphere is stiff in both coordinates as the cylinder with the same radius is in the meridional coordinate. This is the ultimate reason of use of domes in compression drivers. In these devices it is very common the use of titanium, beryllium, or other stiff and lightweight materials.

Since the dome do not bend, but the suspension does, the stresses on the dome are of the in-plane type, and the suspension's stresses are of bending nature. Figure 9 depicts the two principal stresses S1 and S2 on the dome and the suspension. In the figure we can see the stresses for the upward stroke, being compressive the suspension rim in contact with the dome in the S1 direction, which is radial. However the stress S2 (which is circumferential) is tensile in the dome rim, with less strength than S1. Both S1 and S2 are contour stresses one meridional and one tangential. The meridional bending stress on suspension and the in plane stresses on the dome have an inner stress belt on the inner suspension and a tensile stress belt on the dome rim respectively.

Observe in the figure as well, that the boundary of the two jointed slender bodies has a high concentration of shear forces, as it must be, because the close proximity of compression and extension forces. Scales on the left side must be taken as relatives as in the previous and following examples.

Observe in Figure 10, which represents the principal stresses on the dome and suspension on the downward stroke. For this stroke, the principal stress S1 (meridional) is compressive on the dome rim, and the principal stress S2 is tensile in the inner suspension rim. The path of shear forces is very similar to the one in Figure 9. Both stress S1 and S2 for the upward stroke and the downward stroke have a hoop path, and all stress is concentrated at the interface of the dome and the suspension. Maximum S1 compressive stress is at the suspension's side for the upward stroke, while stress shift to the dome side for the downward stroke. Maximum tensile stress of the S2 component is at the dome side for the upward stroke, while stress shift to the suspension's side for the downward stroke.

To resume, stresses in both directions are sharp circle contours on the suspension and dome rim. This circumstance suggests that these stresses are the cause of the subharmonics that these devices radiate often. In reference [10] it is proposed that the subharmonic generation was caused by the parametric interaction of modes, some of them were localized basically on the dome itself, and some were localized in the suspension. One parametric force is the change of a parameter periodically in a moving assembly or suspension contour with a frequency which is double to the one of an eigenvalue. If the stress of the inner suspension contour is changed periodically twice in a cycle, for example, then a parametric excitation of a suspension mode can be realized. These analyses of the static stresses suggest to the reader a deeper insight of the problem of subharmonic generation.

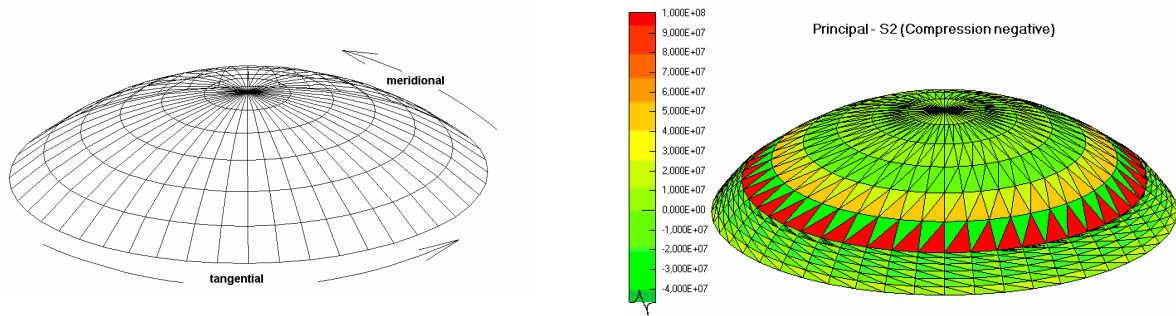


Figure 7: Spherical segment and coordinates.

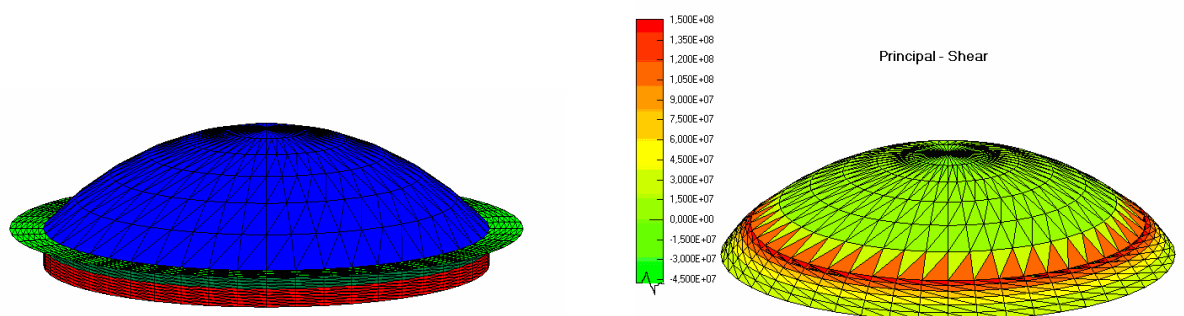
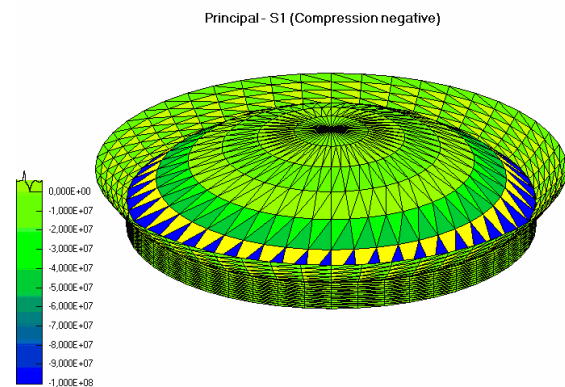
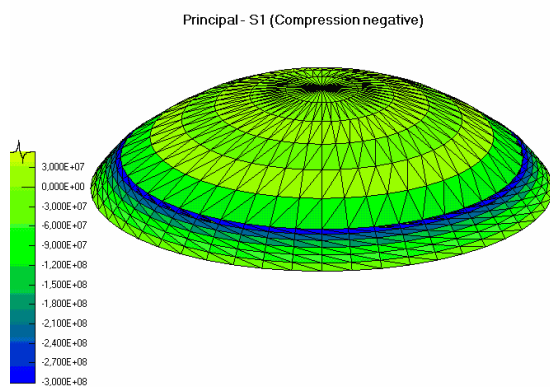


Figure 8: Moving assembly of a compression driver suspended by a flat suspension.

Figure 9: Principal stresses and shear on the dome and suspension of the moving assembly of Figure 8 while it is statically loaded upward. Scales on left are arranged for black and white print, colors not appearing at the model as been erased on the scale.



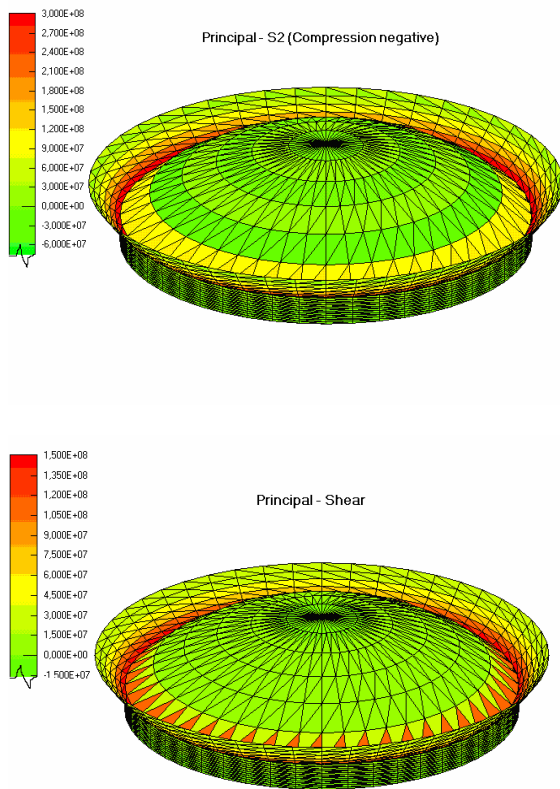


Figure 10: Principal stresses and shear on the dome and suspension of the Figure 8 while the transducer is statically loaded downward.

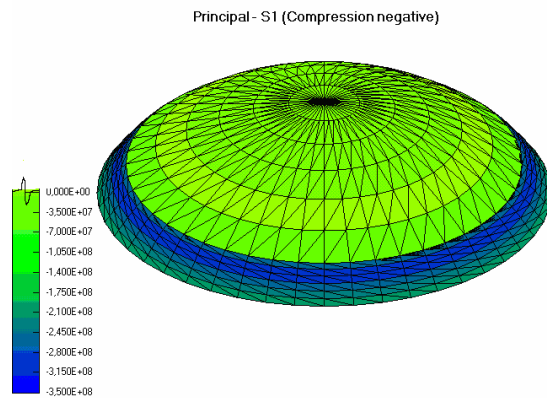
### 3. 1. Nonlinear static analysis of the dome and suspension set.

If we submit the model to the same loads as in linear analysis but applying it in substeps, and each substep is applied to the precedent deformed body. Then a nonlinear analysis of the stiff type is possible. The out-of-plane stiffness of a structure can be significantly affected by the in-plane stress on the structure. The coupling between in-plane stress and transverse stiffness is known as “stress stiffening effect”. For stiff materials like the titanium we are using in the example, polyester, etc., this effect is very common in practice.

Using the same loads, both for the positive and negative stroke, and splitting the load in five

substeps; we find for the flat suspension we are using, a high stress stiffening effect. In linear analysis 10 Newton applied to the coil gives a displacement of 1.573 mm, while the nonlinear analysis in five substeps gives a displacement of only 0.587 mm. These values, despite the high differences found, seem to be realistic.

In Figure 11 the obtained principal stresses S1 and S2 for the upward stroke are depicted, and Figure 12 depicts the principal stresses for the downward stroke. Observe the nonlinear analysis gives stress contours near the same regions that the linear analysis does, but now, both strokes develop compression in the suspension, being the most important the meridional direction. Notice in Figure 12 how S1 has the higher compressive value in the suspension, while in linear analysis was tensile stress and of lesser strength. Observe as well that compressive stress in the suspension after the nonlinear analysis, takes place in both principal stress axis S1 and S2. Finally, notice that the width of compressive span is much higher than the one found in S1 for the upward stroke and linear analysis. These stresses with the same sign in both strokes mean that, if the transducer performs nonlinear, twice in an oscillation cycle, there is a compressive action done in the suspension, which is one of the necessities for a parametric action to create subharmonics. Another necessity mentioned on the reference [10] is the nonlinearity as well.



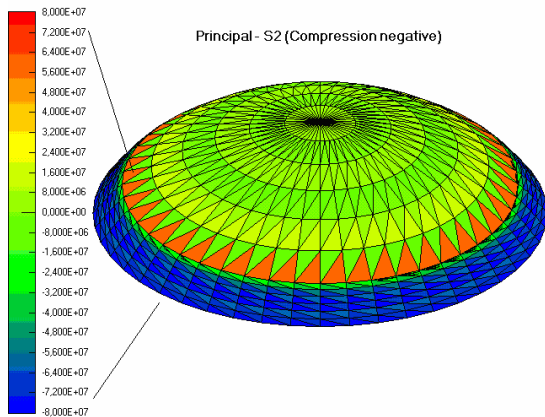


Figure 11: Principal stresses on the dome and suspension of the Figure 8 while the transducer is nonlinear statically loaded upward. Observe the compression all over the suspension.

Figure 12: Principal stresses on the dome and suspension of the Figure 8 while the transducer is nonlinear statically loaded downward. Observe the compression all over the suspension for the upward stroke.

#### 4. THE COMPRESSION STRESSES

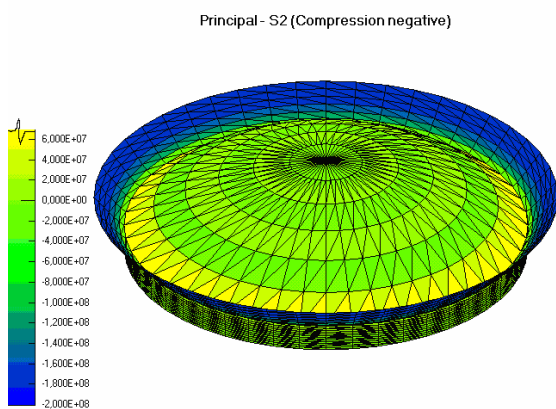
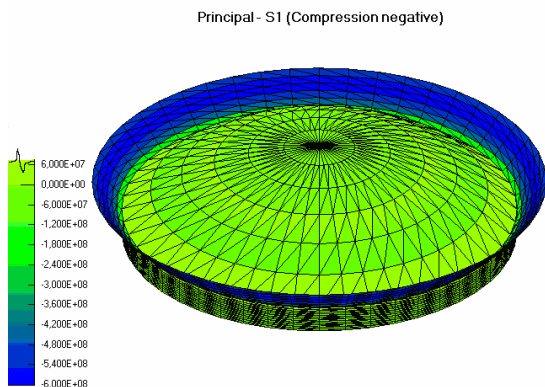
The loudspeaker industry usually works with medium stiffness materials such as the paper pulp, high stiffness materials such as titanium, berilium, etc., and deals very often with materials that have a reasonably tensile stiffness and very small compression stiffness. The technical resinous fabrics are materials that belong to this group of elements without the capacity to handle compression loads. When resinous technical textiles are in compression they normally buckle and wrinkle. These materials are not able to handle these loads.

In engineering, the tensile stress is often preferable to compressive, because any slender body subjected to compressive forces (or temperature) will buckle sooner or later. The buckle theory is based on the Euler's theory, which is reported in [1], [2] and [3]; and more detail for plates and shells in references [4] and [5] for example.

If we imagine a slender column loaded axially, if certain conditions of eccentricity of the load to the column, or other geometrical small imperfections occurred, then the column would bend or buckle for a certain critical load. The buckle is a sudden bending of the column, it is a bending snap.

The Euler's load is inversely proportional to the square of the column length, for this reason the column length is the most important parameter for the critical load. This critical load is the one needed for producing the sudden snap. Figure 13 depicts a spring buckled by an axial load applied to it. The spring deforms axially, but for a certain load, which is the critical load, snaps or bends suddenly as the figure shows. Figure 13 illustrate a slender column axially loaded and buckled to the right.

In Figure 13 the spring has bent to the left because the compressive load and the imperfection of the spring tend to bend to this side, but if the



imperfection was in another physical place the bending would be to other side. An imperfection is any small eccentric loading, small lack of column's orthogonality, etc., Details of this are outside the overall scope of the paper. See the references [4] and [8] for this subject. The buckling problem in shells has been treated widely in bibliography, references [15] and [16] are two of the many.

In textile suspensions, the buckle is very important because any compression load will tend to cause this effect, and the material does not have the capacity for supporting such compressive loads. This circumstance affects very much the performance of the speaker.

Technical textiles perform as soft nonlinear materials, because the interlaced yarns (warp and weft) generally have difficulties to handle shear forces, because the lack of material between yarns and yarn, and because the slippage, among other causes. This soft behaviour, instead of the "stress stiff effect" we have mentioned before, it tend to deliver a large stroke. Some suspensions overcome these difficulties by means of a large amount of resin in the holes between yarns. See, for example, the references [11], [12], [13] and [14].

The Euler's column of Figure 13 buckles bending while it is compressed by in-plane forces acting axially. This implies the simple Euler's column has a bending mode, which will be the final state of the column. Additionally an axial load introduces the in-plane compressive forces in the column. The simplest way to see the process is to assume we have two orthogonal modes one with small amplitude but high compressive stress (column compression), and the other with high displacement (column bending). There are many working structures which are actually in post buckling state, because, some elements have reached this state, but the global structure is able to handle the load. The ultimate strength of an structure, is the maximum load that this structure can handle after the collapse.

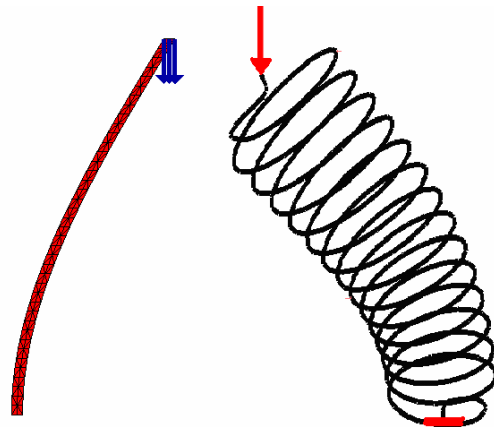


Figure13: The bent Euler's column and a buckled spring after axial compression. Observe how the slender bodies yield on the first bending mode.

In the suspension's field it is common to work with arches. Arches are generally divided in two groups: high arches and shallow arches. High arches are those for which the center line of the arch may be considered incompressible. Flat or shallow arches are those for which its shortening is important. This definition applies for beam arches, and can be applied for shells as well.

Equation (11) changes from beams to high arches taking the form:

$$M / EI = d^2 w / ds^2 + w / R^2 \quad (13)$$

Being  $s$  the coordinate along the arch, and  $R$  the arch radius. The rest of symbols are those given already. Equation (13) explains that the applied bending moment changes the angle of the arch (this will be seen later) and the vertical displacement but affected by the square of the arch radius.

Arches buckles as any slender body does. Figure 14 depicts a problem solved by Timoshenko, which is a shallow arch hinged at both ends, one end by rollers, and uniformly loaded. The figure illustrates the most common state after the critical load is reached, which is the buckling, see [4]. Observe the buckled mode shape which corresponds to the second bending mode.

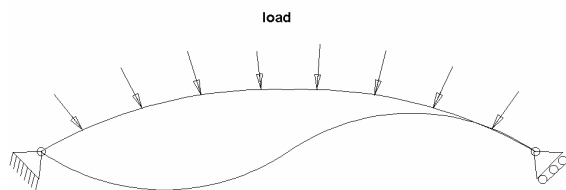


Figure 14: Basic buckle mode in a shallow arch hinged at both ends and loaded uniformly. Observe the arch, after buckling, yields on the second bending mode.

Equation (13) takes the following form for shells of only one curvature as a cylinder.

$$d^2w/ds^2 + w = M * R^2 / D \quad (14)$$

And the equation (13) has the following solution, which is the same as for rings:

$$w = C_1 * \sin \theta + C_2 \cos \theta \quad (15)$$

Being the constants  $C_1$  and  $C_2$ . These constants are calculated from the shell's boundary conditions.

The Euler's critical load has a more precise expression for plates, this was due to Bulson [24]. For a square plate made by an orthotropic material this expression is:

$$P_{crit} = 4\pi^2 \sqrt{D_x D_y} / l^2 \quad (16)$$

Being  $l$  the length of the square plate and  $D_x$  and  $D_y$  the bending stiffness of the shell in the  $x$  and  $y$  directions respectively, see equation (10).

A better prediction of the critical load takes into account the plate aspect ratio. This aspect ratio is important in buckling processes and modifies the equation (16). Aspect ratio has the form:

$$\phi = d/l * (D_x / D_y)^{1/4} \quad (17)$$

Being  $d$  the plate length and  $l$  the plate width. The aspect ratio plays a significant role in loudspeaker's suspensions. A detail of that topic is beyond the paper's scope.

## 5. COMPRESSIVE LOADS IN A SUSPENSION. THE JUMP IN A SPEAKER

Loudspeaker suspensions buckle as well as other slender bodies do. Buckling is the most common cause of the sudden jump of the working point. The jump phenomenon in speakers was reported in early 1940 by H. Olson [17]. The problem has been treated experimentally in 1976 by Weaver and Leach [18]. Various authors have treated the subject taking the speaker as a whole body with nonlinearities in the suspensions or in the magnetic field, see for example [19], [20] and [21]. The Mowry's approach in reference [22] is done by means of structural analysis.

As already established Euler's column is activated by two modes: the first carrying force (axial and compressive) and small displacement; and the second high transverse displacement and small force; in the speakers we have an equivalent scenario. The main force is exerted by a suspension's radial mode or by radial compressive stress in a suspension's contour. The mode of high compliance is, obviously, the main mode of the speaker, which is the most stable and flexible. When the radial stress exceeds the Euler's critical load, the cone buckles in its softer orthogonal (to the radial force) mode which is the main speaker mode, and the cone jumps.

Here the problem is treated through two examples by means of the statics. Figure 15 depicts a sector of a double half roll suspension, this suspension is common in woofers. The nodes marked on the figure has a correlative identification number. Nodes are numbered from 1 at the speaker frame to 43 at the cone rim. This model has been tested both with a spider and suspension, and as a single suspension unit (without the spider). The results do not change substantially, and the complete suspension is reported here. Applying load to the coil, the linear analysis shows the following details. First, a substantial part of the suspension is in compression, as Figure 16 depicts in the radial stress component. This is the

cause of the buckling and jump the speaker does while it is vibrating at high amplitudes. The vertical node displacement plot of Figure 17 shows that around the nodes 10 and 34, where compression is significant, the suspension has maximum axial displacement, while the nodes in the center of the suspension have a small displacement, and the nodes at the suspension's beginning (frame) and end (cone rim) have almost zero vertical displacement.

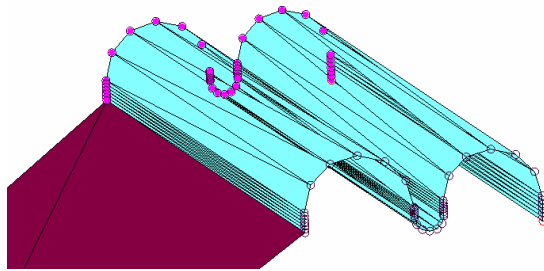


Figure16: Detail of compressions on the suspension. The upper right part of each roll, marked with arrows, is in compression. The intense blue is marked with the b letter (for black and white print).

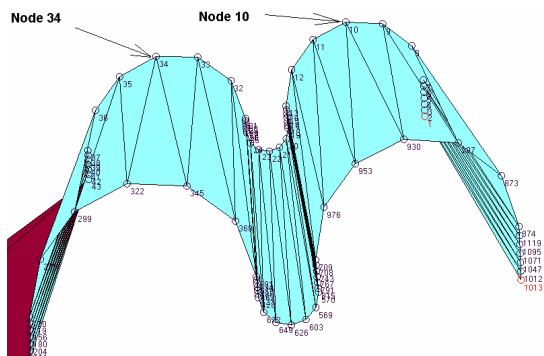
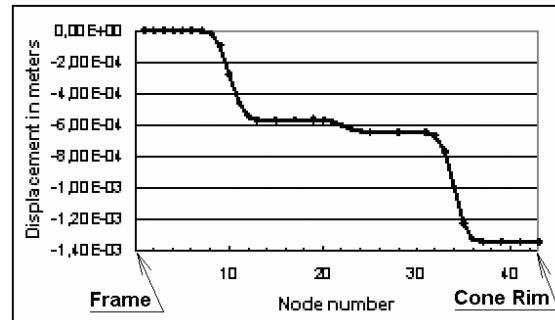


Figure17: Detail of the vertical displacement of each node of Figure 15. Observe the non uniform displacement of the nodes.

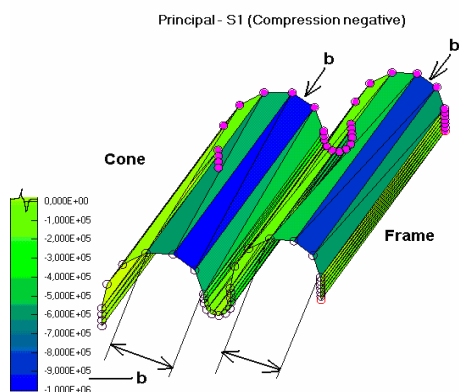
Figure15: Detail of a piece of a double half roll suspensions. On upper figure a set of contour nodes is displayed. In lower figure the nodes 10 and 34 on roll's top are displayed.

In Figure 18 the node rotation and the curvature for each node are depicted. Rotation is given in respect to the Z axis which is normal to the plane of the inset in figure.

Curvature of a curved structure  $\kappa$  is defined (see for example the reference [3]) as the inverse of the radius of curvature  $\rho$ , and has the value:

$$\kappa = 1/\rho = d\theta/ds \quad (14)$$

Observe how in the figure that nodes 10 and 34, have a high rotation and how curvature change their signs in these nodes. This curvature shape indicates that, in both rolls, at the left of the nodes 10 and 34 we have positive curvature and at the right negative curvature. The vertical displacement and the curvature show that the suspension is performing the jump we have seen very often on the speakers at large strokes. However it is convenient to keep in mind that the compression band depicted in Figure 16 is the main cause for this buckling effect.



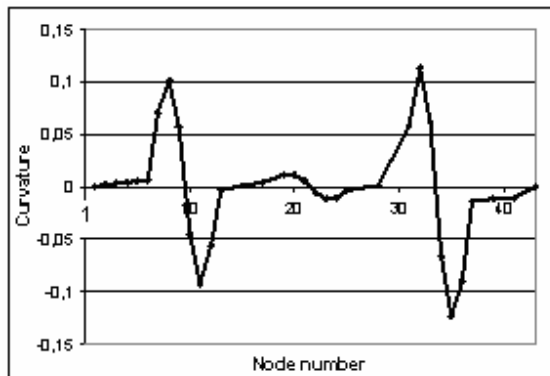
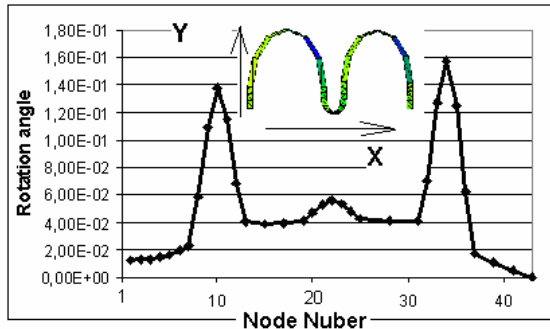


Figure18: Upper: Rotating angle of the nodes and the reference axis in the inset. Rotation is taken respect to the Z axis. Lower : Curvature of the nodes.

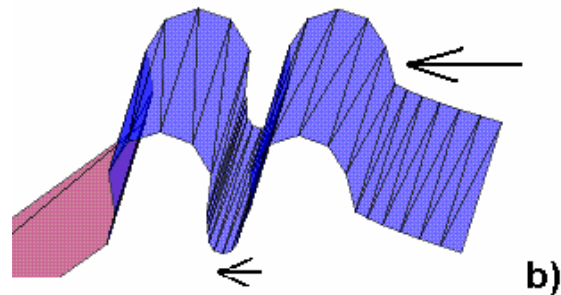
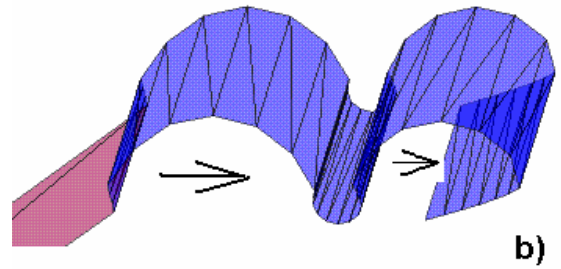
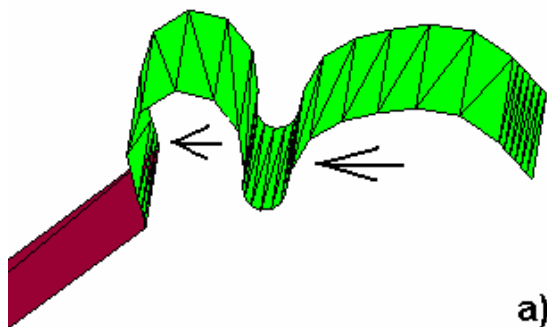
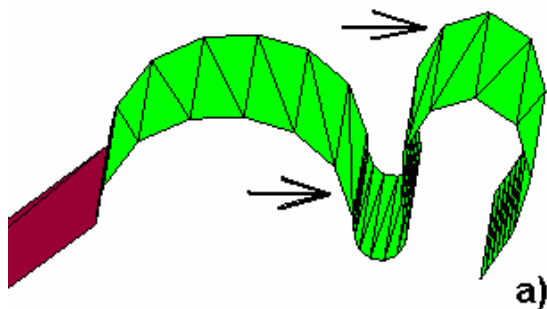


Figure19: Upper a): Hoop suspension’s mode. “Radial” Suspension’s buckling mode. Lower b): Only the pure radial component of this mode. See appendix for details of the hoop modes.



The compressive stress on the suspension can interact with the suspension’s radial mode, which is a hoop mode. At this mode the suspension performs as a bellows that open and closes radially. Figure 19 depicts this mode, observe that while the suspension is in this mode a certain axial motion is allowed in the suspension rim. While suspension is opening, the inner half roll is becoming a shallow arch (shallow half roll), and the outer half roll a high arch (high half roll). The lower figure illustrate only the pure radial component of this mode (the axial motion is restrain and hence, not allowed).

In reference [9] a radial mode was defined in another way, because the definition was based on a cone’s modes, and these modes were defined a long time ago by McLachlan [26]. In fact this mode is a suspension’s hoop mode or an axisymmetric mode. These axisymmetric modes are divided in symmetric and antisymmetric modes. This point is explained in the following example and in the appendix as well.

For a single half roll suspension the situation is similar to the one mentioned above. Figure 20 depicts a moving assembly provided with this suspension. After loading the coil downward we have the principal stress S1 depicted in Figure 21, where we see the compression band on the suspension, from the center to the frame approximately. Figure 22 depicts the vertical displacement and the curvature of all nodes. Similarly to the previous example, the suspension has the maximum vertical displacement on the central band of the roll. The curvature shown in Figure 22, presents a concave and a convex shape from node 1 to node 7. Notice these curvatures are similar to the ones shown for the shallow arch loaded uniformly by a radial pressure and depicted in Figure 14. The curvature of the shallow arch is due to the mode-shape of the second mode of the arch. However the vertical displacement and the curvature of the half roll suspension are due to the interaction of the two involved buckling modes. The main buckling mode is the speaker's main mode, the second buckling mode is a radial (hoop) mode, which is more implicated with the compressive stress. Figure 23 depicts the hoop mode of the suspension. This mode is explained in the appendix. The hoop mode is an axisymmetric mode of the suspension. The hoop mode allows a certain axial displacement. If the axial motion component is restrained we obtain only the symmetric part of this mode, which is depicted on the same figure. The jump of the speaker with two suspensions, which is the most common, has additional complications, but it is based on the same principles described here. Jumps of single suspension's speakers have been described by Klippel [23]. He explained this has been measured even in very small transducers.

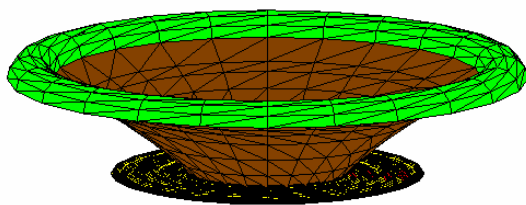


Figure20: Single half roll suspension with the cone and spider.

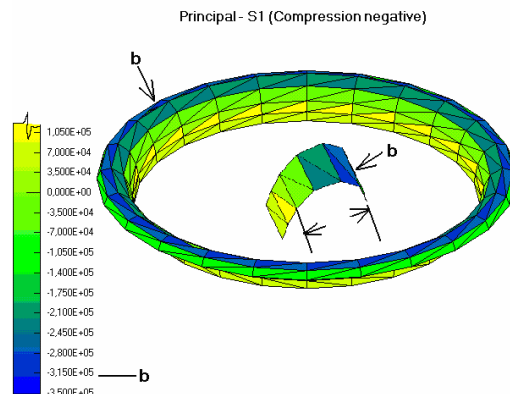


Figure21: Single half roll suspension showing the compression with detail on the inset. The intense blue is marked with the b letter (for black and white print).

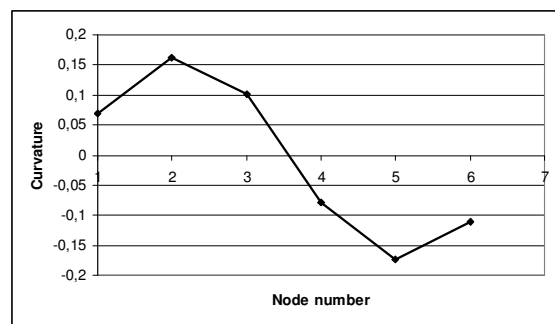
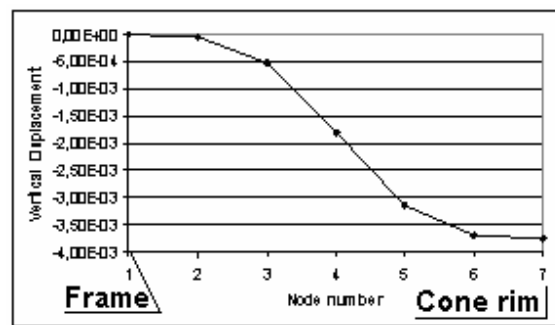


Figure 22: Upper: Vertical displacement of the nodes. Lower: Nodes curvature.

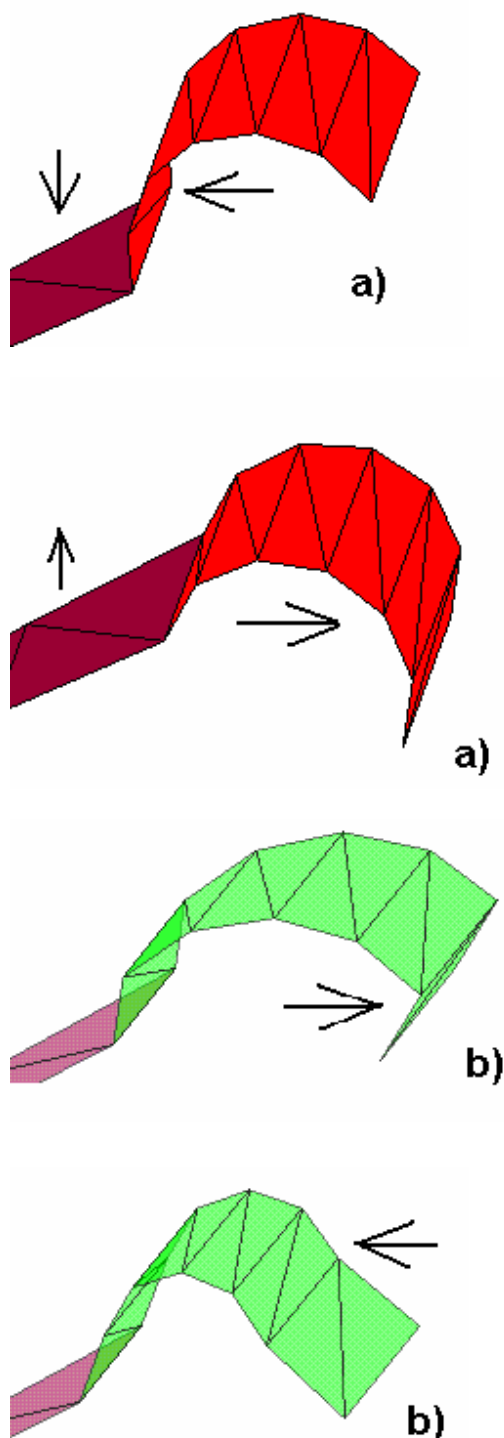


Figure23: Upper a): Hoop (axisymmetric) suspension's mode. Observe the associated axial

displacement. Lower b): Symmetric part of the mode (see appendix).

### 5. 1. Some explanations about multi-arch suspensions behavior.

There are several reasons to manufacture suspensions with multi-arches. A significant cause is the design purpose to obtain a very soft suspension device in the axial direction, and very stiff in radial direction. This is the case of most spiders. The centering task of the spider demands this specific performance.

Other reasons are more or less evident for the reader in respect to reaching targeted design capabilities. However one reason not reported in literature is the advantage these suspensions types give respect to the buckling process.

Multi-roll suspensions improve the compression bands distribution over the full suspension. The compressed bands become distributed in various rolls, instead to be concentrated in the same band of a single or double roll. On the other hand, these bands have less compressed width than an equivalent suspension with a single half roll or the double roll shown before. The compression width is essential, because Euler's law of buckling establishes that the critical load is inversely proportional to the square of the full compressed span (the compression width).

Figure 24 depicts a stress distribution in a multi-roll spider. Observe the compression bands are distributed along the whole suspension and observe these bands are narrow. This is the cause that multi-roll suspensions have fewer tendency to buckle that single or double half rolls.

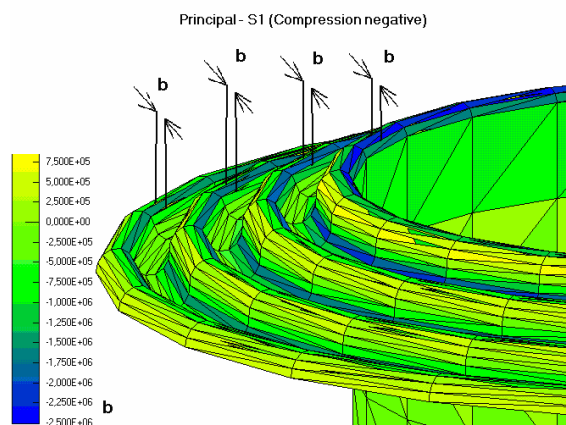


Figure24: Spider deformed upward, showing the narrow compression bands distributed concentrically roll by roll. For black and white print b means intense blue color (high compression).

### 6. EVIDENCE OF BENDING AND IN PLANE STRESS ON SPEAKER'S SUSPENSIONS

It was established in paragraph 1.1 that slender bodies once loaded will experience bending strain and stress when the load is applied, and the in-plane strain and stress will appear further. This was explained in a simplified manner by the example of the hose submitted to water pressure. Because the property that bending of slender shells can be seen easily by rotation, this can be visualized by means of a set of pins or needles.

Figure 25 depicts a spider with two circumferential arrays of pins glued on the inner roll and on the outer roll. The pins are glued on top of the inner and outer rolls. The upper figure shows the unload spider, and the lower figure depicts the loaded spider (with a rather small weight). The bending (curvature) on the inner roll is evident, meaning that in the load process, the inner rolls bends and the outer roll exerts in-plane stress because they do not bend. A basic idea of the sequence of bending and in plane stresses during the loading process can be seen loading the spider further and measuring or evaluating the angles of the pin arrays.

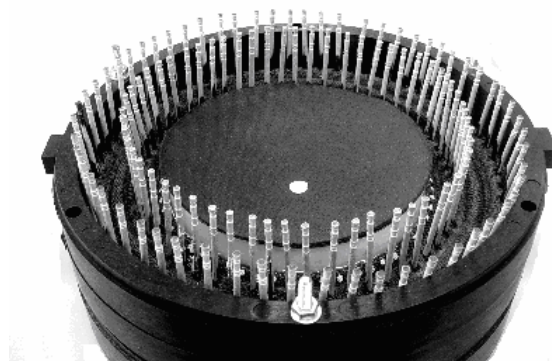


Figure25: Upper: Unloaded spider. Lower: Loaded spider showing the bending strain on the inner roll and in plane strain on the outer roll. The contour of inner pins bents and the outer pins remain still.

Figure 26 depicts a similar set up of three needles glued on a radius of a spider. The upper figure depicts the spider without load. In the lower figure we can see the rotation of the three needles once the spider is loaded with a rather small load. The figure demonstrated that a small load exerts bending in all the spider's rolls of this particular specimen. The initial bending response delivers angles that go from the highest value at inner roll (needle 1) to the lowest at outer roll (needle 3).

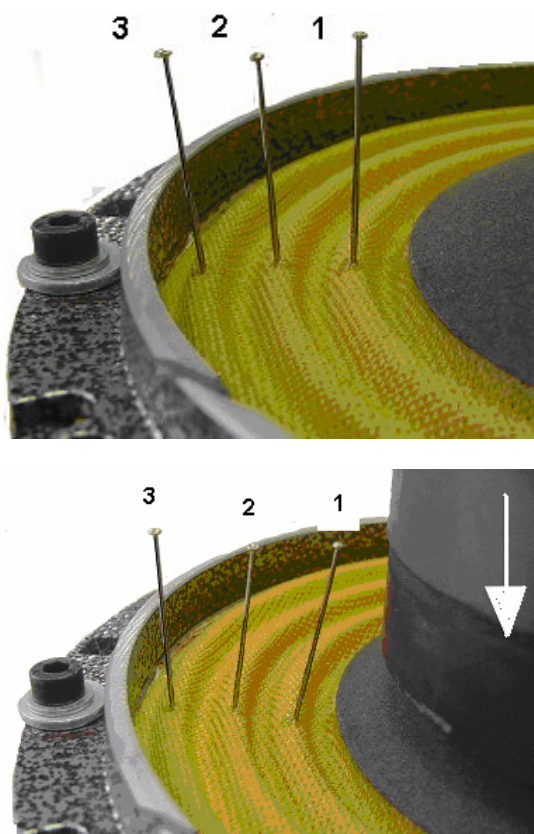
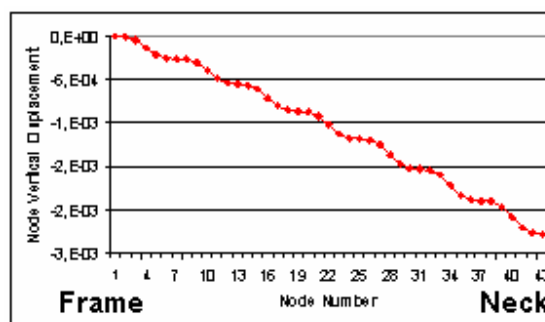


Figure26: Upper: Unloaded spider with needles glued to the rolls. Lower: Spider showing the gradual bending from the inner roll to the outer roll by means of the variation of needle's angle when load is applied.

Vertical node displacement of the spider cross section of Figure 24 is depicted on the upper Figure 27; compare these results with those of Figure 17, where we saw axial displacement jumps. The node rotation in the Z axis (as in the ones of Figure 18) of this spider is depicted in dotted lines in the lower part of Figure 27. The illustrated results are for the downward stroke. The continuous curve of this lower figure represents the vertical coordinate of the spider multiplied by ten. The geometry addition in the plot improves the physical understanding of data. Rotation gives an idea of the bending of all nodes. The results are represented on a wrap form, following the elements local coordinate system. Rotation of nodes in a linear analysis shows a smooth slope along the spider cross section and a small "rotation drift", which is represented by the dotted line. This rotation

drift has only 2 degrees along the full spider span. Between two close roll maxima there is a rotation of 12 degrees approximately, which implies a rotation of 36 degrees for the full spider span. For this particular spider the linear analysis establishes that the bending (rotation) is almost uniform and smooth along the full span. This result fits, to some extent, with the angles we saw in Figure 26 by means of the additional needles for visual verification, but the visual inspection illustrated in Figure 26 gives a higher bending of the inner roll than the middle and outer roll has. It is common, especially in spiders of small size, to find experimental rotations that agree with the theoretical uniform rotation depicted in Figure 27, all over the cross section. The experimental demonstration of Figure 26 with higher rotations at the rolls of less radii than the rolls of higher radii is common as well. In practice there is a wide results scatter due to several circumstances. Among the many, there is a wide scatter of geometries and materials, and the problem has been treated here as linear. The problem accepts an stress analysis using only the bending terms of the mathematical evaluation procedure, and the comparison with the results using all terms, as was done in paragraph 2. But this point is not included in order to keep the paper short.

Even though the results are given in the element's local or regional coordinate system a better understanding of the results can be found in the sketch of the model's orientation surfaces as depicted in Figure 28. If both, the closed surface a), and the open surface b) were oriented to the same point (on figure's top), the shell's orientation signs would be the ones shown in the figure. Rotations versus nodes depicted in Figure 27 are those obtained at each node, for the local coordinate system, while sweeping the upper side of the shells b) of Figure 28.



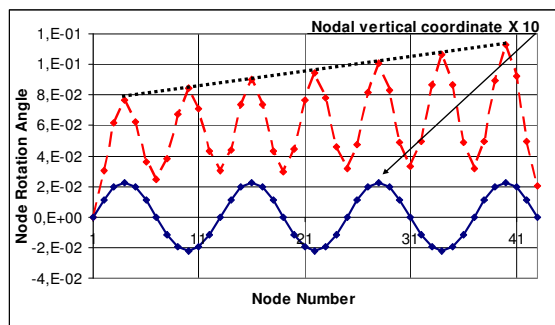


Figure27: Upper node displacement downward. Lower: Node rotation (dotted curve) of the spider of Figure 24. Node 1 belongs to the frame and node 43 belongs to neck. Continuous curve is the vertical coordinate of spider multiplied by 10.

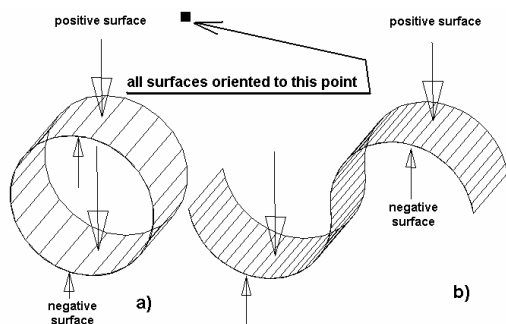


Figure28: Surfaces orientation for signs on the Finite element models. a) closed shell. b) opened shell.

## 7. CONCLUSIONS

A short revision of the tensile and compressive stresses on moving assemblies of speakers has been presented, with special attention to the in-plane and bending stresses.

The problem of subharmonic generation in some dome and suspensions of compression drivers, has been treated by the nonlinear loading of the transducer in both strokes. The compressive stress

concentration on the suspension's contours in both strokes reveals that there is a parametric action that justifies this acoustic radiation. The method of static analysis is much simpler than the modal method.

Finally, the same procedures applied for cones and domes demonstrates that the jump phenomenon in a loudspeaker is basically due to the buckling of its suspensions, due to the compression stresses that appears on wide bands (rings) of them. The paper describes the modes interacting on this buckling process. One of these modes is the main axial mode of the speaker, the second mode is one hoop mode of the suspension. Stress analysis together with the nodes displacements and rotation gives a clear picture of the buckling and structural behavior of the moving assemblies and suspensions. The advantage of multi roll suspensions respect to the one half roll and two half rolls has been treated as well.

## APPENDIX: THE HOOP MODES

Reference [25] analyzes the modal analysis of an inflated torus. This paper gives an overview of this axisymmetric slender body. Due to the fact that the half roll suspension derives from a torus, it is interesting to note two important axisymmetric modes that this body has. Figure A1 depicts one of these modes, which is called the symmetric mode. The mode is called symmetric because it yields a symmetric picture of a meridional cross section. Figure A2 depicts the antisymmetric mode for a torus. Similarly this axisymmetric antysymmetric mode yields an antisymmetric picture of a meridional cross section of the torus. The depicted mode shape corresponds to a torus both inflated and in depressurized state as well. Reference [25] studies the influence of the torus aspect ratio on the natural frequencies of the antisymmetric and symmetric axisymmetric modes. Torus aspect ratio is based on the relationship  $r/R$ , being  $r$  the cross section radius and  $R$  the torus radius.

Observe how the modes depicted on Figures 19 and 23 are hoop modes of their respective suspensions. The depicted mode shape of the upper parts of figures 19 and 23 was the antisymmetric part, and the modes depicted on bottom of these figures are the symmetric part of these suspension's modes. The antisymmetric

part is the one which has higher interaction of the mode with the regular axial speaker mode. The symmetric part is more independent and has less capacity of interaction with the main speaker mode. However, due to the coupling to the cone, in practice it is more common to have antisymmetric modes than symmetric ones.

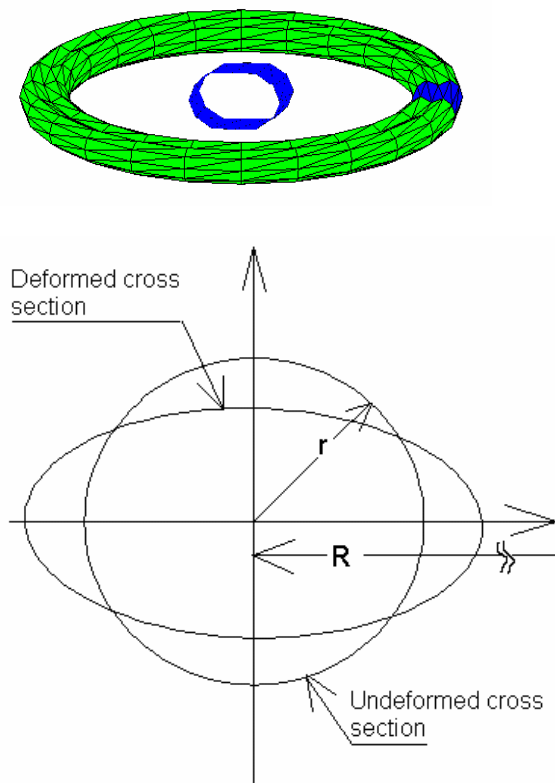


Figure A1: Hoop suspension's mode in a torus. Symmetric mode of the two axisymmetric modes of the torus. Bottom figure depicts the undeformed and the deformed cross section.

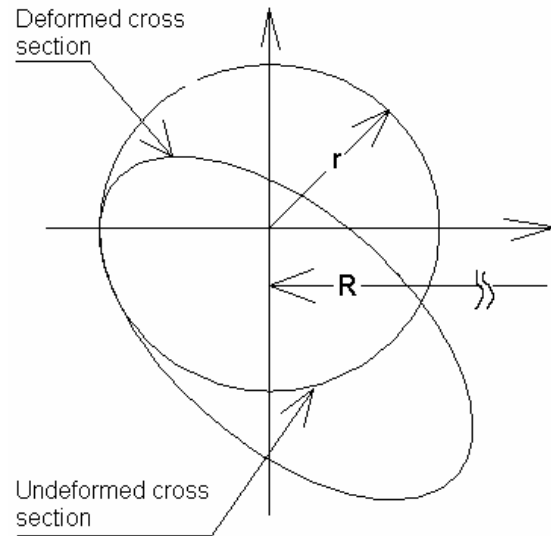
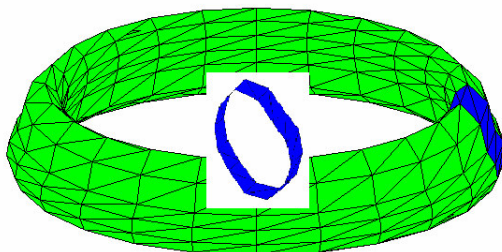


Figure A2: Hoop suspension's mode in a torus. Antisymmetric mode of the two axisymmetric modes of the torus. Bottom figure depicts the undeformed and the deformed cross section.

## 8. REFERENCES

- [1] J. P. Den Hartog, *Advanced Strength of Materials*, Dover Publication, 1987. First published by Mac Graw Hill in 1952.
- [2] W. A. Nash, *Strength of Materials*, Mac Graw Hill, 1969.
- [3] J.M. Gere, *Mechanics of Materials 5th*, Brooks Cole, 2001.
- [4] Z.P. Bazant and L. Cedolin, *Stability of Structures*, Dover Publications, 2003.
- [5] J. Barbe, *Structures Coques, Equations Generales and Stabilité*, Ecole National Supérieure de l'aéronautique et de l'espace, 1980.
- [6] W.M. Jenkins, *Matrix and Digital Computers Methods in Structural Analysis*, Mac Graw Hill, 1969.

- [7] J.S. Przemieniecki, Theory of Matrix Structural Analysis, Mac Graw Hill, 1968.
- [8] C.L.Dym, Stability Theory and its applications to structural mechanics, Dover Publications 1974.
- [9] F. Bolaños, Modal Analysis and Nonlinear Normal Modes (NNM) on Moving Assemblies of Loudspeakers, AES 119<sup>th</sup> Convention, New York, October 2005.
- [10] F. Bolaños, Measurement and Analysis of Subharmonics and Other Distortions in Compression Drivers, AES 118<sup>th</sup> Convention, Barcelona, May 2005.
- [11] J. Domskienè and E. Strazdienè Investigation of Fabric Shear Behaviour, Fibres and Textiles in Eastern Europe, Vol 13, N° 2, April - June 2005, Available in internet.
- [12] P.Xue, X. Peng and J. Cao, A non orthogonal constitutive model for characterizing woven composites, Composites: Part A, Vol. 34, pp 183 – 193, 2003.
- [13] X. Q. Peng, J. Cao, Numerical Determination of Mechanical Elastic Constants of Textile Composites, 15<sup>th</sup> Annual technical Conference of the American Society for Composite, College Station, TX, September 2000.
- [14] Various authors. See on the web <http://www.dir.de/fa/publikationen/>
- [15] G.W. Hunt and G.J. Lord and M.A. Peletier, Cylindrical Shell Buckling: A Characterization of Localization and Periodicity, Discrete and Continuous Dynamical Systems- Series B; Volume 3 Number 4 November 2003.
- [16] A. Spagnoli, Different Buckling Modes in Axial Stiffened Conical Shells, Engineering Structures, Vol. 23, pp 957-965, 2001.
- [17] H. F. Olson, Acoustical Engineering, Professional Audio Journals Inc., 1991. First published as: Elements of Acoustical Engineering, D. Van Nostrand Co. Inc., 1940
- [18] J. E. Weaver and W. M. Leach, Optical Measurement of Loudspeaker Driver Large Signal Displacement Parameters. 55<sup>th</sup> AES Convention, October 29- November 1, 1976.
- [19] A. Dobrucki, Constant Component of the Loudspeaker Diaphragm Displacement Caused by Nonlinearities. 84<sup>th</sup> AES Convention, Paris, March 1-4, 1988.
- [20] A. Dobrucki, Nontypical Effects in an Electrodynamic Loudspeaker with a Nonhomogeneous Magnetic Field in the Air Gap and Nonlinear Suspensions. J. Audio Engi. Soc., Vol 42, 7/8, July /August 1994.
- [21] A. Jabbari and A. Unruh, Jump Resonance in Audio Transducers, 117<sup>th</sup> AES Convention, San Francisco, October 2004.
- [22] S. Mowry, Searching for Soft-Part Linearity, on: <http://s-m-audio.com/>.
- [23] W. Klippel, Large Signal Performance of Tweeters, Microspeakers and Horn Drivers, 118<sup>th</sup> AES Convention, Barcelona, May 2005.
- [24] P. S. Bulson, The stability of flat plates, American Elsevier Publishing Co., New York, 1969.
- [25] A.K. Jha, D. J. Inman, R. H. Plaut, Free Vibration Analysis of an Inflated Toroidal Shell, Journal of Vibration and Acoustics, Vol. 124, July 2002.
- [26] N.W. McLachland, Loudspeakers: Theory, Performance, testing and design, 1934, Oxford University Press.